

# Synthesis, Characterization, and Electrochemical and Electrical Properties of Novel Pentaerythritol-Bridged Cofacial Bismetallophthalocyanines and Their Water-Soluble Derivatives

Metin Özer,<sup>[a]</sup> Ahmet Altındal,<sup>[b]</sup> Ali Rıza Özkaya,<sup>[a]</sup> Bekir Salih,<sup>[c]</sup> Mustafa Bulut,<sup>[a]</sup> and Özer Bekaroğlu\*<sup>[d]</sup>

**Keywords:** Phthalocyanines / Cofacial configuration / Synthesis / Cyclic voltammetry / Thermopower

Novel cofacial bismetallophthalocyanines and their water-soluble derivatives were prepared. The precursor 4,4'-(2-phenyl-1,3-dioxane-5,5-diyl)bis(methylene)bis(oxy)diphthalonitrile **3** was obtained by the reaction of [5-(hydroxymethyl)-2-phenyl-1,3-dioxan-5-yl] methanol **1** and 4-nitrophthalonitrile **2** with K<sub>2</sub>CO<sub>3</sub> in DMF at 50 °C. Cyclotetramerization was achieved by heating the homogenized mixture of the precursor, bisphthalonitrile, and Zn(OAc)<sub>2</sub>·2H<sub>2</sub>O or Co(OAc)<sub>2</sub>·4H<sub>2</sub>O at 300 °C, which was followed by catalytic hydrogenation of the resulting product with Pd/C(10%) in DMF. The target water-soluble phthalocyanines were acquired from boiling suspensions of the compounds bearing eight OH side groups in aqueous KOH (20%) solution. The structure of the target compounds was confirmed by elemental analysis, FTIR, UV/Vis, <sup>1</sup>H NMR, ICP-MS, and MALDI-TOF spectroscopic methods. The electrochemical and spectroelectrochemical measurements suggested the formation of

various mixed-valent oxidation and reduction species, as a result of the strong intramolecular interactions between the two cofacial phthalocyanine units in the compounds. Impedance spectroscopy, dc conductivity, and thermopower measurements were performed using spin-coated films of these compounds as a function of temperature (290–440 K) and frequency (40–10<sup>5</sup> Hz). Dc conductivity showed typical Arrhenius behavior for all compounds. At low temperatures, a curved line was observed for the complex plane plots of impedance for all phthalocyanines. These curved lines transformed into a full semicircle with increasing temperature. The dependency of frequency exponent *s* on temperature suggested hopping-type conduction. A positive Seebeck coefficient was observed for all compounds, which indicates that the compounds behave as a *p*-type semiconductor. (© Wiley-VCH Verlag GmbH & Co. KGaA, 69451 Weinheim, Germany, 2007)

## Introduction

Phthalocyanine (Pc) dimers and multimers have been the subject of great interest in areas such as electrocatalysis,<sup>[1,2]</sup> semiconductors,<sup>[3]</sup> nonlinear optics,<sup>[4]</sup> electrochromic displays,<sup>[5–7]</sup> and liquid crystals.<sup>[8,9]</sup> In this respect, various phthalocyanine,<sup>[10–12]</sup> porphyrin,<sup>[13,14]</sup> and mixed phthalocyanine-porphyrin dimers and oligomers<sup>[15]</sup> having various kinds of linkage have been reported to date. These compounds, especially those with rigid cofacial configurations,<sup>[16,17]</sup> often show spectroscopic, electrical, and electrochemical properties which differ significantly from the parent monomers. A strong interaction between the face-to-face Pc rings or two metal centers in these types of com-

plexes was usually detected with spectroscopic and electrochemical evidence.<sup>[18]</sup>

Thin films of organic molecular crystals are promising materials for electronic and optoelectronic devices like solar cells,<sup>[19]</sup> gas sensors,<sup>[20]</sup> and light-emitting diodes<sup>[21]</sup> due to their unique electrical properties. The determination of true fundamental parameters such as the majority carrier type and electronic structure is crucial in order to optimize their potential utility for optical or electronic applications. Optical methods such as ultraviolet photoemission and inverse photoemission spectroscopy are used to determine the electronic structure of phthalocyanine thin films.<sup>[22]</sup> On the other hand, Hall effect and thermopower measurements are used for the determination of the charge carrier type. The most reliable method to investigate their conduction type is the measurement of thermoelectric power, characterized by the Seebeck coefficient *S*.

The synthesis and properties of cofacial bismetallophthalocyanines with a number of cross-links have been rarely reported in the literature.<sup>[23,24]</sup> Our interest in the design of novel macrocycles with potential applicability in various technological areas prompted us to synthesize new bridged metallated bisphthalocyanines with four linking

[a] Department of Chemistry, Marmara University, Istanbul, 34722, Turkey

[b] Department of Physics, Marmara University, Istanbul, 34722, Turkey

[c] Department of Chemistry, Hacettepe University, Ankara, 06532, Turkey

[d] Department of Chemistry, Istanbul Technical University, Maslak-Istanbul, 34469, Turkey  
Fax: +90-216-3860824  
E-mail: obek@itu.edu.tr  
obekaroglu@gmail.com

arms between two Pc rings and to investigate their electrochemical and electrical properties.<sup>[18,25]</sup> Recently, we reported the synthesis, characterization, and electrical and spectroelectrochemical properties of 1,1'-methyleneindaphthalene-bridged cofacial metal-free bisphthalocyanines and bismetallophthalocyanines.<sup>[18]</sup>

In our continuing efforts, we now report the synthesis and characterization of novel pentaerythritol-bridged cofacial bismetallophthalocyanines and their water-soluble derivatives. The electrochemical and electrical properties of the compounds are also investigated.

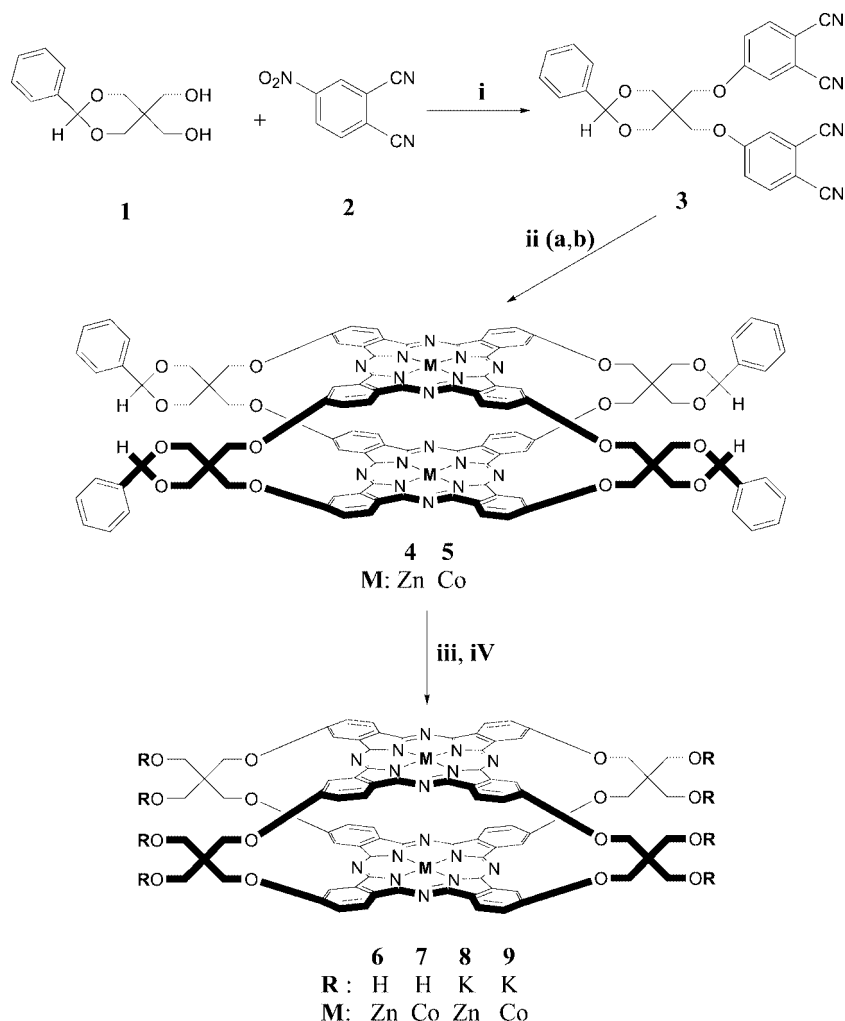
## Results and Discussion

### Synthesis

The preparation of the pentaerythritol monoacetal **1** was accomplished by the condensation of pentaerythritol with benzaldehyde in DMF at 25–30 °C according to the given method.<sup>[26,27]</sup> The original precursor **3** for the synthesis of phthalocyanines was obtained by nitro displacement reaction of **1** and **2** using  $K_2CO_3$  as catalyst in DMF with stir-

ring at 50–60 °C. In this work, for the synthesis of the cofacial bismetallophthalocyanines, we developed a solid-phase method in the absence of catalysts. The preparation of phthalocyanine derivatives **4** and **5** was achieved by heating the homogenized mixture of **3** with  $Zn(OAc)_2 \cdot 2H_2O$  or  $Co(OAc)_2 \cdot 4H_2O$ , respectively, in the ratio 1:1 through the cyclotetramerization reaction in a sealed tube at 300 °C for 10 min. The mixtures of Pc **4** or **5** and Pd/C(10%) in DMSO were hydrogenated at room temperature under 1 atm hydrogen pressure for 8 h according to the given procedure.<sup>[27]</sup> The catalyst was filtered off, and the mixtures were precipitated with the addition of ethanol to give Pc **6** or **7**. Water-soluble Pcs **8** and **9** were achieved by boiling suspensions of **6** or **7**, respectively, in aqueous KOH (20%) solutions (Scheme 1).

The crude Pcs **4–7** were dissolved in DMF and precipitated again with a mixture of  $CHCl_3$  and ethanol which easily dissolved the starting material and the other impurities. After filtration, each precipitate was washed with boiling acetone and ethanol. The purification of the target Pcs **4–7** was achieved with a silica gel column using a THF/DMF gradient system as the eluent. On the other hand, **8**



Scheme 1. (i)  $K_2CO_3$ , DMF; (ii) a:  $Zn(CH_3COO)_2 \cdot 2H_2O$ , b:  $Co(CH_3COO)_2 \cdot 4H_2O$ ; (iii)  $H_2$ , Pd/C(10%); (iv) KOH (20%).

or **9** were dissolved in water, and they were precipitated again several times in ethanol until the solution was neutral. The precipitates were washed with ethanol and diethyl ether, and then dried in vacuo.

After purification, the compounds were characterized by elemental analysis, FTIR,  $^1\text{H}$  NMR, UV/Vis, MALDI-MS, and ICP-MS spectroscopy. The results of the analyses showed that the compounds were pure enough for the other measurements.

The IR spectra were derived from potassium bromide disks. The existence of  $\text{C}\equiv\text{N}$  groups appeared at  $2231\text{ cm}^{-1}$  as a single peak in the spectrum of **3**. Formation of dinuclear phthalocyanine complexes **4** and **5** starting from the corresponding bisphthalodinitrile derivative was verified by the disappearance of the  $\text{C}\equiv\text{N}$  stretching vibration band at  $2231\text{ cm}^{-1}$ . After conversion of **4** and **5** into **6** and **7**, respectively, by the cleavage of the acetal groups, O–H stretching vibrations came out typically around  $3402$  and  $3396\text{ cm}^{-1}$  as strong absorptions.

The UV/Vis spectra of **4–7** in DMF display characteristic absorptions around  $625$  and  $680\text{ nm}$  in the Q-band region (Figure 1). The Q-band was attributed to  $\pi \rightarrow \pi^*$  transition from the highest occupied molecular orbital (HOMO) to the lowest unoccupied molecular orbital (LUMO) of the Pc ring. The other bands (B) in the UV region at  $330\text{--}353\text{ nm}$  are observed due to the transitions from the deeper  $\pi$  levels to the LUMO. When aggregation occurs, a band at ca.  $630\text{ nm}$  arises in the electronic spectrum as a result of the intramolecular interactions between the Pc units.<sup>[18,28]</sup> Thus, the band at around  $625\text{ nm}$  can be attributed to intramolecular interactions, although the Q-band is not split. The aggregation degree of Pcs is highly affected by the surrounding conditions, one of which is the solvent media. Figures 2 and 3 show the absorption spectra of water-soluble Pcs **8** and **9**, respectively, at different concentrations [ $C_8 = (5.28 \times 10^{-6})\text{--}(4.8 \times 10^{-7})$  and  $C_9 = (7.52 \times 10^{-6})\text{--}(8.22 \times 10^{-7})$ ]. It should be noted that the absorption at around  $630\text{ nm}$ , corresponding to aggregation, for **8** and **9** is the main band in water.<sup>[29]</sup> This observation suggests that aggregation occurs to a greater extent in water as compared with that in organic solvent.<sup>[30,31]</sup> In addition, although the concentrations of dinuclear water-soluble phthalocyanines **8** and **9** decrease, there is no significant change in the relative intensity of the aggregation band to the Q-band at ca.  $685\text{ nm}$ . This situation is consistent with the intramolecular coupling between the rings in dinuclear phthalocyanines.

In addition to these results, the  $^1\text{H}$  NMR ( $[\text{D}_6]\text{DMSO}$ ) spectra of **3**, **4**, and **6** exhibit the characteristic chemical shifts for the proposed structures as expected. The  $^1\text{H}$  NMR spectrum of **6**, the hydrogenolysis product of **4**, provides supporting evidence for the structure. Removal of the benzylidene acetal in **4** is confirmed by the loss of the singlet proton signal of acetal at  $\delta = 6.14\text{ ppm}$  in the  $^1\text{H}$  NMR spectrum of **6**. A broad signal at  $\delta = 11.35\text{ ppm}$  in the  $^1\text{H}$  NMR spectrum of **6** disappeared with  $\text{D}_2\text{O}$  exchange. The  $^1\text{H}$  NMR spectra of **3**, **4**, and **6** exhibit the aromatic protons as multiplets at  $7.73\text{--}7.21$ ,  $8.42\text{--}7.03$ , and  $8.31\text{--}6.94\text{ ppm}$ , respectively. On the other hand, aliphatic proton signals ap-

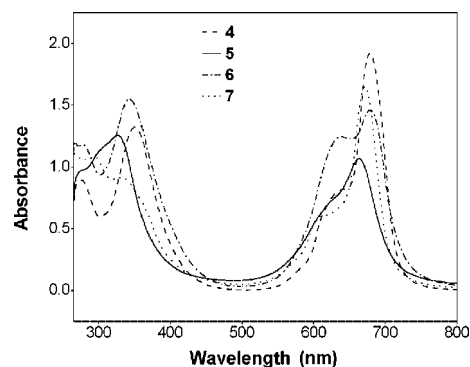


Figure 1. UV/Vis spectra of bis(metallophthalocyanine) derivatives **4–7** in DMF.

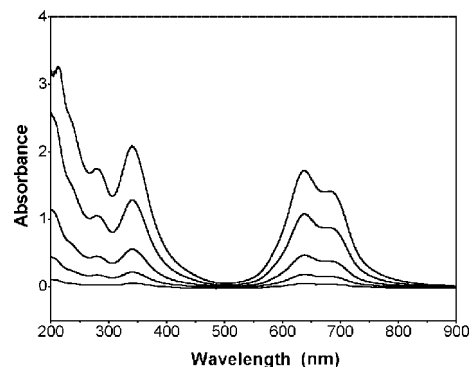


Figure 2. UV/Vis spectra of bis(metallophthalocyanine) derivative **8** in water at different concentrations.

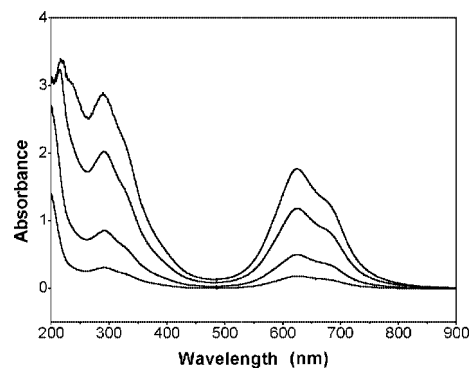


Figure 3. UV/Vis spectra of bis(metallophthalocyanine) derivative **9** in water at different concentrations.

peared at  $4.88\text{--}3.64\text{ ppm}$  for **3**,  $4.81\text{--}3.57\text{ ppm}$  for **4**, and  $4.12\text{--}3.13\text{ ppm}$  for **6**.

A close investigation of the MALDI-TOF mass spectra of the Pcs confirmed the proposed structures. The protonated molecular ion peaks of **4** and **5** are observed at low intensity, but sodium adduct peaks for both **4** and **5** complexes are found to be dominant intense peaks in the linear mode MALDI-TOF mass spectra using the 3-indoleacrylic acid matrix. Sodium adduct peak stabilities of these complexes were found to be very high in the gas phase compared to the stability (following the intensity of the peaks) of the protonated molecular ion peaks, even if the sodium content in the complexes was lower than  $0.1\%$  (data not

shown). On the other hand, protonated molecular ion peaks of **6** and **7** complexes are observed at 1685 and 1672 Da, respectively, which exactly overlap with the mass of the protonated complexes calculated from the elemental composition of the compounds. Following the protonated molecular ion peak of **6**, a peak, 88 Da mass lower than the protonated molecular ion peak, is observed at 1596 Da. This peak resulted from the  $C_4H_8O_2$  side group elimination from the protonated ion peak of the complex. Also the second  $C_4H_8O_2$  side group elimination is observed at low intensity. However, no fragmentation was observed for **7** in the MALDI-TOF mass spectrum. When the MALDI-TOF mass spectra of **6** and **7** were evaluated at low-mass range between 100 and 500 Da, no meaningful intensity peak was observed representing impurities, but mainly matrix species peaks were followed. These results show that either **6** or **7** complexes were very pure. Many different MALDI matrices were tested to obtain highly resolved spectra. The best matrix for **6** and **7** was  $\alpha$ -cyano-4-hydroxycinnamic acid for MALDI-MS analyses. Because of the short life time of the protonated complexes **6** and **7** in MALDI-MS, highly resolved spectra could not be obtained in reflectron mode. Beyond the protonated and two fragment ion peaks of **6** and the only protonated ion peak of **7**, MALDI mass spectra of the complexes showed very clear and low fragmentations in MALDI-MS (Figures 4 and 5).

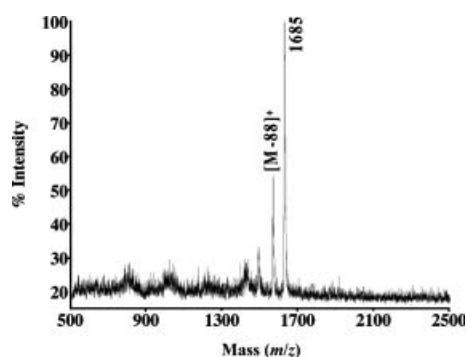


Figure 4. Positive ion mode MALDI-MS spectrum of **6** in  $\alpha$ -cyano-4-hydroxycinnamic acid MALDI matrix using nitrogen laser accumulating 50 laser shots.

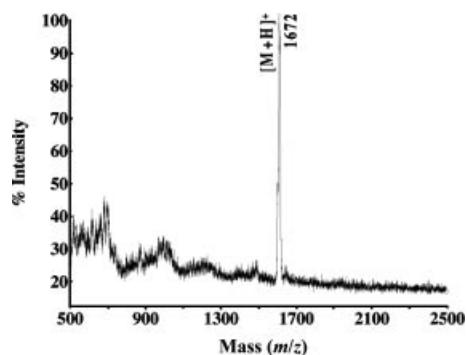


Figure 5. Positive ion mode MALDI-MS spectrum of **7** in  $\alpha$ -cyano-4-hydroxycinnamic acid MALDI matrix using nitrogen laser accumulating 50 laser shots.

The ICP-MS measurements were obtained for the determination of the quantities of potassium, zinc, and cobalt atoms in **8** and **9** as described in the literature.<sup>[32]</sup> The results of ICP-MS analysis provide additional support for the molecular structures of **8** and **9**.

### Electrochemistry and Spectroelectrochemistry

The electrochemical properties of the complexes **4–7** were examined by cyclic voltammetry, controlled potential coulometry, and spectroelectrochemistry in DMSO/TBAP. Cyclic voltammetry of each complex displayed four reductions and an oxidation couple. Typical cyclic voltammograms of **4** and **5** in DMSO/TBAP (tetrabutylammonium perchlorate) are shown in Figure 6. The number of electrons transferred for each redox process is determined by the controlled potential electrolysis at the suitable potentials. Coulometric studies of broadly separated voltammetric couples showed that the number of electrons transferred for each redox process ( $p$ ) is approximately equal to unity ( $1 > p \geq 0.92$ ). Thus, the reactions corresponding to all waves in the voltammograms are stepwise one-electron processes of the two cofacial phthalocyanine rings and metal centers. The voltammetric data and the assignment of the redox couples for **4–7** are summarized in Table 1. The occurrence of stepwise one-electron processes for these complexes involving two Pc rings and two metal centers, and the comparison of their half-peak potentials with those of monophthalocyanines imply the formation of mixed-valent first- and second-reduced and first-oxidized species during the voltammetric measurements.<sup>[33,18]</sup> It can be concluded from the results of this study that the binding of two Pc rings at two sides rigidly with four linking arms leads to remarkable intramolecular cofacial coupling and thus to the splitting of the classical monophthalocyanine redox processes. For instance, for complexes **4** and **6**, the  $Pc(-2)/Pc(-3)$  redox process is split into the  $[Pc(-2)]_2/[Pc(-2) \cdot Pc(-3)]$  and  $[Pc(-2) \cdot Pc(-3)]/[Pc(-3)]_2$  processes, forming the mixed-valent  $[Pc(-2) \cdot Pc(-3)]$  species. All the redox processes for **4** and **6** should be ligand-based since the  $Zn^{II}$  ion is not redox-active in metallophthalocyanines. The difference between the first oxidation and the first reduction potentials for complexes **4** and **6** is remarkably low relative to that of monophthalocyanines (1.34 V for **4**, 1.33 V for **6**, but 1.50–1.70 V for monophthalocyanines). This is in harmony with the cofacial structures of **4** and **6**, leading to the strong electronic coupling and the splitting of molecular orbitals. Previous reports on the electrochemistry of  $Co^{II}$  Pcs suggested that both the first reduction and the first oxidation processes in these complexes are metal-based in polar coordinating solvents such as DMSO and DMF.<sup>[32]</sup> Since complexes **5** and **7** involve two  $Co^{II}$  centers, the oxidation and the first two reductions probably correspond to  $[Co^{II}Pc(-2) \cdot Co^{III}Pc(-2)]^+ / [Co^{II}Pc(-2)]_2$ ,  $[Co^{II}Pc(-2)]_2 / [Co^{II}Pc(-2) \cdot Co^I Pc(-2)]^-$ , and  $[Co^{II}Pc(-2) \cdot Co^I Pc(-2)]^- / [Co^I Pc(-2)]_2^{2-}$  redox processes, respectively. On the other hand, the third and fourth reductions should be related to the splitting of the  $Pc(-2)/Pc(-$

(–3) couple and thus ligand-based  $[\text{Co}^{\text{I}}\text{Pc}(-2)]_2^{2-}/[\text{Co}^{\text{I}}\text{Pc}(-2)\cdot\text{Co}^{\text{I}}\text{Pc}(-3)]^{3-}$  and  $[\text{Co}^{\text{I}}\text{Pc}(-2)\cdot\text{Co}^{\text{I}}\text{Pc}(-3)]^{3-}/[\text{Co}^{\text{I}}\text{Pc}(-3)]_2^{4-}$  redox processes, respectively.

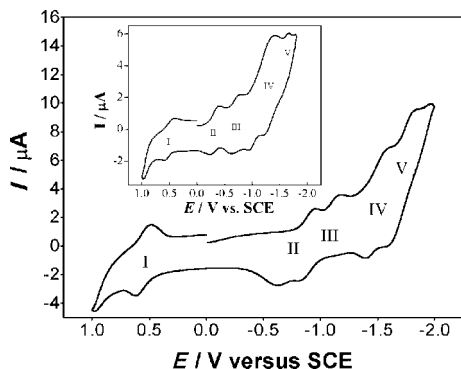


Figure 6. Cyclic voltammograms of **4** and **5** (inset) at 0.100 V/s in TBAP/DMSO.

Table 1. Electrochemical data for **4**–**7** in DMSO.<sup>[a]</sup>

Pc Redox processes		$E_{1/2}$ [V]	$\Delta E_p$ [V]	$\Delta E$ [V]	$\Delta E_s$ [V]	
<b>4</b> $[\text{Zn}(\text{II})\text{Pc}(-2)\cdot\text{Zn}(\text{II})\text{Pc}(-1)]^+ / [\text{Zn}(\text{II})\text{Pc}(-2)]_2$	I	0.55	0.12	1.34	0.21	
	$[\text{Zn}(\text{II})\text{Pc}(-2)]_2 / [\text{Zn}(\text{II})\text{Pc}(-2)\cdot\text{Zn}(\text{II})\text{Pc}(-3)]$	II	–0.79			0.30
	$[\text{Zn}(\text{II})\text{Pc}(-2)\cdot\text{Zn}(\text{II})\text{Pc}(-3)] / [\text{Zn}(\text{II})\text{Pc}(-3)]_2^{2-}$	III	–1.00			0.32
	$[\text{Zn}(\text{II})\text{Pc}(-3)]_2^{2-} / [\text{Zn}(\text{II})\text{Pc}(-3)\cdot\text{Zn}(\text{II})\text{Pc}(-4)]^3$	IV	–1.47			0.18
	$[\text{Zn}(\text{II})\text{Pc}(-3)\cdot\text{Zn}(\text{II})\text{Pc}(-4)]^3 / [\text{Zn}(\text{II})\text{Pc}(-4)]_2^{4-}$	V	–1.71			0.22
<b>5</b> $[\text{Co}(\text{II})\text{Pc}(-2)\cdot\text{Co}(\text{III})\text{Pc}(-2)]^+ / [\text{Co}(\text{II})\text{Pc}(-2)]_2$	I	0.50	0.18	0.80	0.43	
	$[\text{Co}(\text{II})\text{Pc}(-2)]_2 / [\text{Co}(\text{II})\text{Pc}(-2)\cdot\text{Co}(\text{I})\text{Pc}(-2)]^-$	II	–0.30			0.16
	$[\text{Co}(\text{II})\text{Pc}(-2)\cdot\text{Co}(\text{I})\text{Pc}(-2)]^- / [\text{Co}(\text{I})\text{Pc}(-2)]_2^{2-}$	III	–0.73			0.12
	$[\text{Co}(\text{I})\text{Pc}(-2)]_2^{2-} / [\text{Co}(\text{I})\text{Pc}(-2)\cdot\text{Co}(\text{I})\text{Pc}(-3)]^{3-}$	IV	–1.17			0.46
	$[\text{Co}(\text{I})\text{Pc}(-2)\cdot\text{Co}(\text{I})\text{Pc}(-3)]^{3-} / [\text{Co}(\text{I})\text{Pc}(-3)]_2^{4-}$	V	–1.43			0.42
<b>6</b> $[\text{Zn}(\text{II})\text{Pc}(-2)\cdot\text{Zn}(\text{II})\text{Pc}(-1)]^+ / [\text{Zn}(\text{II})\text{Pc}(-2)]_2$	I	0.52	0.14	1.33	0.25	
	$[\text{Zn}(\text{II})\text{Pc}(-2)]_2 / [\text{Zn}(\text{II})\text{Pc}(-2)\cdot\text{Zn}(\text{II})\text{Pc}(-3)]$	II	–0.81			0.32
	$[\text{Zn}(\text{II})\text{Pc}(-2)\cdot\text{Zn}(\text{II})\text{Pc}(-3)] / [\text{Zn}(\text{II})\text{Pc}(-3)]_2^{2-}$	III	–1.05			0.42
	$[\text{Zn}(\text{II})\text{Pc}(-3)]_2^{2-} / [\text{Zn}(\text{II})\text{Pc}(-3)\cdot\text{Zn}(\text{II})\text{Pc}(-4)]^3$	IV	–1.48			0.20
	$[\text{Zn}(\text{II})\text{Pc}(-3)\cdot\text{Zn}(\text{II})\text{Pc}(-4)]^3 / [\text{Zn}(\text{II})\text{Pc}(-4)]_2^{4-}$	V	–1.73			0.22
<b>7</b> $[\text{Co}(\text{II})\text{Pc}(-2)\cdot\text{Co}(\text{III})\text{Pc}(-2)]^+ / [\text{Co}(\text{II})\text{Pc}(-2)]_2$	I	0.48	0.16	0.80	0.26	
	$[\text{Co}(\text{II})\text{Pc}(-2)]_2 / [\text{Co}(\text{II})\text{Pc}(-2)\cdot\text{Co}(\text{I})\text{Pc}(-2)]^-$	II	–0.32			0.16
	$[\text{Co}(\text{II})\text{Pc}(-2)\cdot\text{Co}(\text{I})\text{Pc}(-2)]^- / [\text{Co}(\text{I})\text{Pc}(-2)]_2^{2-}$	III	–0.75			0.34
	$[\text{Co}(\text{I})\text{Pc}(-2)]_2^{2-} / [\text{Co}(\text{I})\text{Pc}(-2)\cdot\text{Co}(\text{I})\text{Pc}(-3)]^{3-}$	IV	–1.20			0.10
	$[\text{Co}(\text{I})\text{Pc}(-2)\cdot\text{Co}(\text{I})\text{Pc}(-3)]^{3-} / [\text{Co}(\text{I})\text{Pc}(-3)]_2^{4-}$	V	–1.46			0.12

[a] Potentials are reported with respect to the SCE. Half-wave potentials in DMSO vs.  $\text{Fc}/\text{Fc}^+$  couple correspond approximately with the given **4**–**7** data minus 0.45 V.  $E_{1/2}$  values were measured by cyclic voltammetry [ $E_{1/2} = (E_{pa} + E_{pc})/2$ ]. The peak separation values ( $\Delta E_p = E_{pa} - E_{pc}$ ) are reported at 0.100 V/s.  $\Delta E$  is the potential difference between the first oxidation and first reduction potentials. It represents the HOMO–LUMO gap for **4** and **6**, but the charge-transfer transition for **5** and **7** involving redox-active metal centers.  $\Delta E_s$  indicates mixed-valent splitting energy for the relevant split redox couple.

The spectroelectrochemical measurements in solution have a vital importance in confirming the assignment of the redox processes in the Pcs, especially in metallo Pcs involving a redox-active metal center. The formation of electro-

chemically generated species involving a  $\text{Co}^{\text{I}}$  center is confirmed by the appearance of a new intense absorption in the region of 400–500 nm. Figure 7 shows in situ UV/Vis spectral changes during the first and second reductions and the first oxidation of **5** in TBAP/DMSO. Upon the first reduction, a new intense band appears at 488 nm, confirming the formation  $\text{Co}^{\text{II}}\cdot\text{Co}^{\text{I}}$  mixed-valent species.<sup>[34,35]</sup> This band can be assigned to metal-to-ligand charge transfer (MLCT) from  $\text{Co}^{\text{I}}$  to the Pc ring. During the second reduction, the absorption of the newly formed MLCT peak continues to increase, forming a quite intense band with a redshift in the Q-band. It is known from the literature<sup>[36,37]</sup> that both  $\text{Co}^{\text{II}}\cdot\text{Co}^{\text{I}}$  and  $\text{Co}^{\text{I}}\cdot\text{Co}^{\text{I}}$  species show Q-band and MLCT absorption (near 500 nm) redshifted relative to less electronically coupled dimers or monophthalocyanines. Thus, the spectral changes observed during the second reduction process indicate the formation of  $\text{Co}^{\text{I}}\cdot\text{Co}^{\text{I}}$  species. The spectrum of the mixed-valent  $\text{Co}^{\text{II}}\cdot\text{Co}^{\text{I}}$  species obtained during the first reduction is different from that of the fully reduced  $\text{Co}^{\text{I}}\cdot\text{Co}^{\text{I}}$  species obtained during the second reduction. The  $\text{Co}^{\text{II}}\cdot\text{Co}^{\text{I}}$  mixed-valent species has a much weaker MLCT band. This implies that the added first electron may be delocalized over the extended ring system. This type of behavior was observed previously for the (–1)-bridged dinuclear  $[\text{CoTRNPc}]_2$  (TRN = trineopentoxy).<sup>[12]</sup> The spectroelectrochemistry of **5** provides additional support for the fact that the reduction of **5** and **7** over the first and second reduction couples proceeds by two distinct one-electron steps, corresponding to the stepwise reduction of each of the cobalt atoms to  $\text{Co}^{\text{I}}$ .

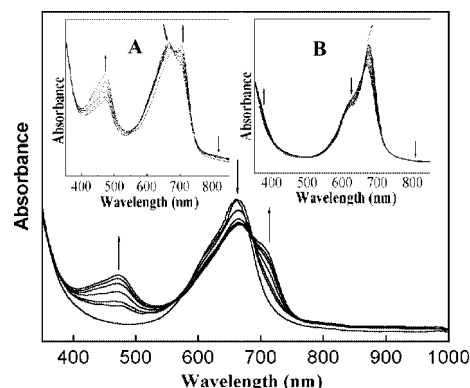


Figure 7. In situ UV/Vis spectral changes during the first reduction, the second reduction (inset A), and the first oxidation (inset B) processes of **5** in TBAP/DMSO.

### Electrical Conductivity and Thermopower Measurements

Dc conductivity of the spin-coated films was determined from the slope of the measured current–voltage ( $I$ – $V$ ) measurements by using the following relation:

$$\sigma_{\text{dc}} = \frac{I}{V(2n-1)lh}$$

where  $I$  is the measured current,  $V$  is the bias voltage,  $d$  is the electrode spacing,  $n$  is the number of electrode finger

pairs,  $l$  is the overlap length of the electrode fingers, and  $h$  is the thickness of the electrodes. Measurements of  $I$ - $V$  were carried out in the range of  $-1$  to  $1$  V. Linear  $I$ - $V$  behavior was found in this voltage range, indicating no rectifying properties. The variation of the measured dc conductivity with temperature suggests the presence of only one conduction mechanism, assuming that the dominant levels are the conduction and valence bands, in the whole temperature range for the films of **4**-**9**. Arrhenius plots (logarithms of dc conductivity versus inverse temperature) indicated that the compounds are semiconducting in nature. The highest value of conduction activation energy was obtained for the film of **8** and the lowest for **5**. The difference between the electrical conductivity of the films can be attributed to the differences in the stacking arrangements and interplanar spacing.

The frequency-dependent conductivity (ac conductivity) measurements were also performed on thin films of compounds in the frequency range  $40$ – $10^5$  Hz at temperatures between  $290$  and  $440$  K. The frequency dependence of the electrical conductivity for a large variety of materials can be expressed as  $\sigma = \sigma_0 + \sigma(\omega)$ , where  $\sigma_0$  is the dc conductivity. The frequency-dependent part of the total conductivity,  $\sigma(\omega)$ , is given by the power law of the form<sup>[38]</sup>  $\sigma(\omega) = A\omega^s$  where  $A$  and  $s$  are temperature-dependent parameters. For temperatures above  $350$  K, frequency-independent conductivity at low frequencies and after a certain characteristic frequency increasing with the power law, was observed. Various models such as tunnelling and hopping have been proposed to explain this type of behavior. It is not easy to decide which of these mechanisms is responsible for the observed conduction mechanism. However, the behavior of the exponent  $s$  with temperature can help in determining the possible conduction mechanism. The values of  $s$  are calculated from the slope of the  $\ln\sigma(\omega, T)$  versus  $\ln\omega$  graphs and were generally found to decrease with increasing temperature. It was observed that the calculated values of the frequency exponent  $s$  are in agreement with the hopping model.

The measured impedance spectra, when plotted in a complex plane plot, appeared in the form of a succession of semicircles representing the contributions to the electrical properties due to bulk material, grain boundary effect, and interfacial polarization phenomena. So, the impedance spectra technique enabled us to separate the effects due to each component. At low temperatures, the impedance spectra consist of a quasivertical line. The existence of semicircular-shaped curves in the Nyquist plot means that the impedance becomes capacitive, even at relatively high frequency. The effect of temperature on the impedance spectra of the films becomes clearly visible with a rise in temperature. On the complex plane plot at high temperatures, only a depressed semicircle with a different radius is observed (Figure 8) for the compounds **4**-**9** at higher temperatures, indicating deviation from the Debye dispersion relation. In the case of a depressed semicircle in the impedance spectra, the relaxation time is considered as a distribution of values, rather than a single relaxation time.

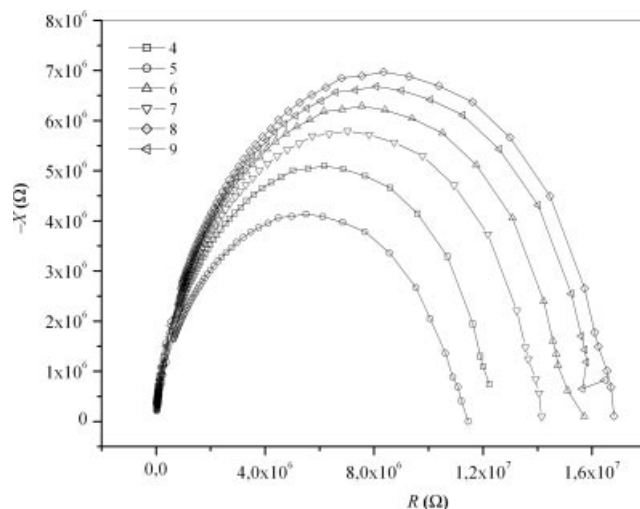


Figure 8. Nyquist plot (imaginary part vs. real part of complex impedance) of the spin-coated films of **4**-**9** at  $385$  K.

The Seebeck coefficient  $S$  provides the transport type by its sign and provides the energetic difference between the Fermi level and transport level by its value. To determine the type of majority carrier, the temperature dependence of the thermoelectric power was also studied for thin films of **4**-**9**. The measured thermopower varied approximately exponentially with temperature for all samples investigated. Figure 9 shows the Seebeck coefficient  $S$  of the samples. Its sign is always positive. Compared to **8**, the absolute value of the thermopower for the film of **5** is larger by nearly a factor of 3. The positive sign of  $S$  confirms that the thin films of the compounds behave as a  $p$ -type semiconductor.

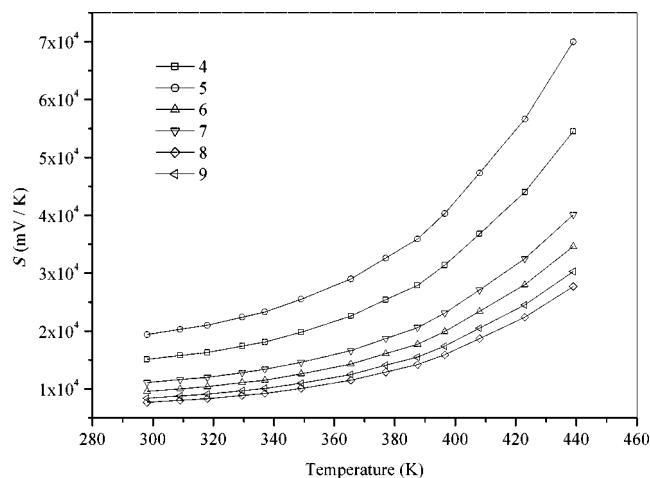


Figure 9. Seebeck coefficient vs. temperature for the films of **4**-**9**.

## Experimental Section

**General:** Compound **1** was synthesized by the methods previously described in the literature.<sup>[21,22]</sup> 4-Nitrophthalonitrile, pentaerythritol, benzaldehyde,  $\text{Zn}(\text{AcO})_2 \cdot 2\text{H}_2\text{O}$ ,  $\text{Co}(\text{AcO})_2 \cdot 4\text{H}_2\text{O}$ , and Pd/C(10%) were obtained from commercial suppliers.

Routine IR and UV/Vis spectra were recorded with a Shimadzu FTIR-8300 spectrophotometer as KBr pellets and with a Shimadzu

UV-1601 UV/Vis spectrophotometer, respectively. Elemental analyses were performed with the LECO CHNS 932.  $^1\text{H}$  NMR spectra were obtained with a Varian Mercury-Vx 400 MHz spectrometer. Mass spectra were acquired with a Voyager-DE<sup>TM</sup> PRO MALDI-TOF mass spectrometer (Applied Biosystems, USA) equipped with a nitrogen UV-Laser operating at 337 nm. Spectra were recorded in linear mode with an average of 50 shots. 3-Indole acrylic acid (IAA) (20 mg/mL in acetonitrile) MALDI matrix for **4** and **5**, and  $\alpha$ -cyano-4-hydroxycinnamic acid (ACCA) (15 mg/mL in 1:1 water/acetonitrile) MALDI matrix for **6** and **7** were prepared. MALDI samples were prepared by mixing the complex (2 mg/mL in dimethyl sulfoxide) with the matrix solution (1:10, v/v) in a 0.5-mL Eppendorf<sup>®</sup> microtube. Finally this mixture (1  $\mu\text{L}$ ) was deposited on the sample plate, dried at room temp. and then analyzed. The potassium, zinc, and cobalt contents in the digested mixtures were determined using external standards with an Agilent 7500a inductively coupled plasma mass spectrometer (ICP-MS). For the ICP-MS measurements, compounds **8** and **9** (10 mg) were digested by a mixture of acids ( $\text{HNO}_3/\text{HClO}_4/\text{HF}$ , 8:2:2, v/v) at 170 °C for 1 h.

**4,4'-(2-Phenyl-1,3-dioxane-5,5-diyl)bis(methylene)bis(oxy)diphthalonitrile (3):** A mixture of **1** (1.79 g, 8 mmol), **2** (2.77 g, 16 mmol), and  $\text{K}_2\text{CO}_3$  (6.62 g, 48 mmol) in DMF (80 mL) was heated with stirring at 50 °C under argon for 30 h. The cooled reaction mixture was poured into cold water (100 mL) with stirring. The formed precipitate was filtered, washed with water, and dried in vacuo. The separation of the prepared compounds was achieved by column chromatography using silica gel with  $\text{CHCl}_3$ . The white powder product was obtained by evaporation of the solvent. This compound is readily soluble in  $\text{CHCl}_3$ ,  $\text{CH}_2\text{Cl}_2$ , acetone, and THF. Yield 1.82 g (48%). M.p. 223 °C.  $^1\text{H}$  NMR ( $\text{CDCl}_3$ ):  $\delta$  = 7.73–7.21 (m, 11 H, arom. CH), 5.51 (s, 1 H, acetal CH), 4.88–3.64 (m, 8 H, aliph.  $\text{CH}_2$ ) ppm. IR (KBr):  $\tilde{\nu}$  = 3074–3038 (arom. CH), 2926–2851 (aliph. CH), 2231 ( $\text{C}\equiv\text{N}$ ), 1595 (arom.  $\text{C}=\text{C}$ ), 1483, 1390, 1309, 1246 (aliph.–O–arom.), 1165, 1093  $\text{cm}^{-1}$ .  $\text{C}_{28}\text{H}_{20}\text{N}_4\text{O}_4$ : calcd. C 70.58, H 4.23, N 11.76; found C 70.81, H 4.29, N 11.62.

**2',10',16',24'-[Tetrakis(2-phenyl-1,3-dioxan-5,5-diyl)bis(methylene)bis(oxy)]bis(phthalocyaninato)dizinc(II) (4) and 2',10',16',24'-[Tetrakis(2-phenyl-1,3-dioxan-5,5-diyl)bis(methylene)bis(oxy)]bis(phthalocyaninato)dicobalt(II) (5):** Compound **3** (0.24 g, 0.5 mmol) and  $\text{Zn}(\text{OAc})_2\cdot 2\text{H}_2\text{O}$  (0.22 g, 1 mmol) or  $\text{Co}(\text{OAc})_2\cdot 4\text{H}_2\text{O}$  (0.13 g, 0.5 mmol) were ground in a mortar. Then the mixture was put in a glass tube, and the tube was purged with argon. After being sealed, the mixture was heated at 300 °C for 10 min. After cooling to room temp., the deep turquoise blue **4** or deep blue **5** were powdered by grinding. The crude products were dissolved in DMF (5 mL) and reprecipitated with a mixture of acetone/ethanol (1:1, v/v). After filtration, the precipitates were washed successively with hot water, ethanol, and acetone, and dried in vacuo. Compounds **4** and **5** were isolated using silica gel and a gradient of THF/DMF (10:0.1 to 10:2, v/v) as the eluent. These compounds are soluble in THF, DMSO, DMF, and DMA. Yield (**4**): 58 mg (23%). M.p. >300 °C. UV/Vis (DMF):  $\lambda$  (log  $\epsilon$ ) = 680 (5.29), 638 (4.92), 353 (5.12) nm (Figure 1).  $^1\text{H}$  NMR ( $[\text{D}_6]\text{DMSO}$ ):  $\delta$  = 8.42–7.03 (m, 44 H, arom. CH), 6.14 (s, 4 H, acetal CH), 4.81–3.57 (m, 32 H, aliph.  $\text{CH}_2$ ) ppm. IR (KBr):  $\tilde{\nu}$  = 3067 (arom. CH), 2926 (aliph. CH), 1607 (arom.  $\text{C}=\text{C}$ ), 1232 (aliph.–O–arom.), 1090, 1065  $\text{cm}^{-1}$ . MALDI-TOF MS:  $m/z$  = 2038  $[\text{M} + \text{H}]^+$ , 2082  $[\text{M} - \text{H} + 2\text{Na}]^+$ .  $\text{C}_{112}\text{H}_{80}\text{N}_{16}\text{O}_{16}\text{Zn}_2$ : calcd. C 66.05, H 3.96, N 11.00; found C 65.84, H 3.89, N 11.12. Yield (**5**): 46 mg (18%). M.p. >300 °C. UV/Vis (DMF):  $\lambda$  (log  $\epsilon$ ) = 665 (5.03), 625 (4.88), 330 (5.10), 278 (4.99) nm (Figure 1). IR (KBr):  $\tilde{\nu}$  = 3045 (arom. CH), 2941–2850 (aliph. CH), 1603 (arom.  $\text{C}=\text{C}$ ), 1265, 1228 (aliph.–O–arom.), 1095, 1057  $\text{cm}^{-1}$ . MALDI-TOF MS:  $m/z$  = 2023  $[\text{M} + \text{H}]^+$ , 2045  $[\text{M} + \text{Na}]^+$ , 2091

$[\text{M} + 3\text{Na}]^+$ .  $\text{C}_{112}\text{H}_{80}\text{Co}_2\text{N}_{16}\text{O}_{16}$ : calcd. C 66.47, H 3.98, N 11.07; found C 67.14, H 4.11, N 11.32.

**2',10',16',24'-[Tetrakis(4,4'-2,2-bis(hydroxymethyl)propane-1,3-diyl)bis(oxy)]bis(phthalocyaninato)dizinc(II) (6) and 2',10',16',24'-[Tetrakis(4,4'-2,2-bis(hydroxymethyl)propane-1,3-diyl)bis(oxy)]bis(phthalocyaninato)dicobalt(II) (7):** A suspension of **4** (0.11 g, 0.06 mmol) or **5** (0.12 g, 0.054 mmol) and Pd/C(10%) (30 mg) in DMSO (20 mL) was hydrogenated at room temp. under 1 atm hydrogen pressure for 8 h. The catalyst was filtered off, and the mixture was precipitated with the addition of ethanol to give **6** or **7**. Compounds **6** or **7** were dissolved in DMF (2 mL) and reprecipitated with a mixture of acetone/ethanol (1:1, v/v). After filtration, the precipitates were washed successively with hot acetic acid, water, and alcohol, and dried in vacuo. The purification of **6** and **7** was carried out using silica gel columns with a THF/DMF system changing from 10:0.1 to 10:1 (v/v). These compounds are soluble in THF, DMSO, DMF, and DMA. Yield (**6**): 69 mg (76%). M.p. >300 °C. UV/Vis (DMF):  $\lambda$  (log  $\epsilon$ ) = 680 (5.08), 639 (5.02), 344 (5.11) nm (Figure 1).  $^1\text{H}$  NMR ( $[\text{D}_6]\text{DMSO}$ ):  $\delta$  = 11.35 (br s, 8 H, aliph. OH, disappeared with  $\text{D}_2\text{O}$  exchange), 8.31–6.94 (m, 24 H, arom. CH), 4.12–3.13 (m, 32 H, aliph.  $\text{CH}_2$ ) ppm. IR (KBr):  $\tilde{\nu}$  = 3402 (aliph. OH), 3059 (arom. CH), 2926–2851 (aliph. CH), 1603 (arom.  $\text{C}=\text{C}$ ), 1466, 1228 (aliph.–O–arom.), 1089, 1045  $\text{cm}^{-1}$ . MALDI-TOF MS:  $m/z$  = 1685  $[\text{M} + \text{H}]^+$ , 1596  $[\text{M} - 88]^+$  (Figure 4).  $\text{C}_{84}\text{H}_{64}\text{N}_{16}\text{O}_{16}\text{Zn}_2$ : calcd. C 59.90, H 3.83, N 13.31; found C 60.44, H 3.79, N 13.63. Yield (**7**): 62 mg (63%). M.p. >300 °C. UV/Vis (DMF):  $\lambda$  (log  $\epsilon$ ) = 674 (5.13), 610 (4.69), 336 (4.88) nm (Figure 1). IR (KBr):  $\tilde{\nu}$  = 3396 (aliph. OH), 3053 (arom. CH), 2933–2874 (aliph. CH), 1603 (arom.  $\text{C}=\text{C}$ ), 1468, 1232 (aliph.–O–arom.), 1094, 1056  $\text{cm}^{-1}$ . MALDI-TOF MS:  $m/z$  = 1672  $[\text{M} + \text{H}]^+$  (Figure 5).  $\text{C}_{84}\text{H}_{64}\text{Co}_2\text{N}_{16}\text{O}_{16}$ : calcd. C 60.36, H 3.86, N 13.41; found C 61.01, H 3.80, N 13.11.

**2',10',16',24'-[Tetrakis(4,4'-2,2-bis(oxidomethyl)propane-1,3-diyl)bis(oxy)]bis(phthalocyaninato)dizinc(II) Octapotassium (8) and 2',10',16',24'-[Tetrakis(4,4'-2,2-bis(oxidomethyl)propane-1,3-diyl)bis(oxy)]bis(phthalocyaninato)dicobalt(II) Octapotassium (9):** Compound **6** (0.034 g, 0.02 mmol) or **7** (0.017 g, 0.01 mmol) was suspended in aqueous KOH solution (20%, 5 mL) and boiled for 10 min. The solution of the compound **8** or **9** was cooled, and the mixture was poured into ethanol (100 mL). The formed precipitate was filtered off, dissolved in water and reprecipitated in ethanol several times until the solution was neutral. The products were then washed with ethanol and diethyl ether, and dried in vacuo. Both compounds are soluble in water at room temp. Yield (**8**): 0.031 g (77%). M.p. >300 °C. UV/Vis (water):  $\lambda$  (log  $\epsilon$ ) = 687 (4.62), 637 (4.70), 338 (4.53) nm (Figure 2). IR (KBr):  $\tilde{\nu}$  = 3061 (arom. CH), 2939–2870 (aliph. CH), 1605 (arom.  $\text{C}=\text{C}$ ), 1489, 1226 (aliph.–O–arom.), 1095, 1044  $\text{cm}^{-1}$ .  $\text{C}_{84}\text{H}_{56}\text{N}_{16}\text{O}_{16}\text{K}_8\text{Zn}_2$ : calcd. C 50.72, H 2.84, N 11.27; found C 51.08, H 2.79, N 11.31. ICP-MS (Zn, K): Anal. calcd. for  $\text{C}_{84}\text{H}_{56}\text{N}_{16}\text{O}_{16}\text{K}_8\text{Zn}_2$ : Zn 6.58, K 15.73; found Zn 6.47, K 15.91. Yield (**9**): 0.013 g (65%). M.p. >300 °C. UV/Vis (Water):  $\lambda$  (log  $\epsilon$ ) = 685 (4.36), 623 (4.47), 279 (4.67) nm (Figure 3). IR (KBr):  $\tilde{\nu}$  = 3067 (arom. CH), 2931–2865 (aliph. CH), 1601 (arom.  $\text{C}=\text{C}$ ), 1482, 1224 (aliph.–O–arom.), 1093, 1047  $\text{cm}^{-1}$ .  $\text{C}_{84}\text{H}_{56}\text{Co}_2\text{N}_{16}\text{O}_{16}\text{K}_8$ : calcd. C 51.06, H 2.86, N 11.34; found C 50.81, H 2.79, N 11.18. ICP-MS (Co, K): Anal. calcd. for  $\text{C}_{84}\text{H}_{56}\text{Co}_2\text{N}_{16}\text{O}_{16}\text{K}_8$ : Co 5.96, K 15.83; found Co 6.07, K 15.79.

**Electrochemistry and Spectroelectrochemistry:** The cyclic voltammetry (CV) and controlled potential coulometry (CPC) measurements were carried out with a Princeton Applied Research Model VersaStat II potentiostat/galvanostat, which was controlled by an external PC and utilized a three-electrode configuration at 25 °C.

The working electrode was a Pt plate with a surface area of 0.10 cm<sup>2</sup>. The surface of the working electrode was polished with a H<sub>2</sub>O suspension of Al<sub>2</sub>O<sub>3</sub> before each run. The last polishing was done with a particle size of 50 nm. A Pt wire served as the counter electrode. Saturated calomel electrode (SCE) was employed as the reference electrode and was separated from the bulk of the solution by a double bridge. The ferrocene/ferrocenium couple (Fc/Fc<sup>+</sup>) was also used as an internal standard. Electrochemical grade tetrabutylammonium perchlorate (TBAP) in extra pure DMSO was employed as the supporting electrolyte at a concentration of 0.10 mol/dm<sup>3</sup>. High purity N<sub>2</sub> was used for deoxygenating the solution at least 20 min prior to each run and for maintaining a nitrogen blanket during the measurements. For CPC studies, Pt gauze working electrode (10.5 cm<sup>2</sup> surface area), Pt-wire counter electrode separated by a glass bridge, and SCE as a reference electrode were used. The spectroelectrochemical measurements were carried out with an Agilent Model 8453 diode array spectrophotometer equipped with the potentiostat/galvanostat and utilized a three-electrode configuration of thin-layer quartz spectroelectrochemical cell at 25 °C. The working electrode was transparent Pt gauze. Pt-wire counter electrode separated by a glass bridge and a SCE reference electrode separated from the bulk of the solution by a double bridge were used.

**Conductivity and Thermopower Measurements:** The electrodes used in the conductivity and thermopower measurements consisted of an interdigital array of metal electrodes photolithographically patterned on pre-cleaned glass substrate. The films were prepared by spin-coating method. The substrate temperature was kept constant at 290 K during deposition of the materials over the electrodes. Dc conductivity and impedance spectra measurements were performed between 290 and 440 K by using a Keithley 617 electrometer. Ac conductivity and impedance measurements were carried out with a Keithley 3330 LCZ meter in the frequency range 40 to 10<sup>5</sup> Hz, in the temperature range 290 to 440 K. Both dc and ac conductivity measurements were performed under 10<sup>-3</sup> mbar in the dark. The conductivity data were recorded using an IEEE 488 data acquisition system incorporating a personal computer. The thermopower was determined independently from the electrical conductivity measurements. Thermopower measurements were carried out on the same samples, which were prepared for electrical conductivity measurements. The Seebeck coefficient *S* was determined by measuring the voltage for a temperature gradient over the samples by using a Keithley 2000 digital multimeter. The temperature difference between the two sides of the film was measured by a Ni/CrNi thermocouple.

## Acknowledgments

This work was supported by the Research Funds of DPT (Project No: 2003K120810) and Marmara University, and partly by the Turkish Academy of Sciences (TUBA).

- [1] N. Kobayashi, P. Janda, A. B. P. Lever, *Inorg. Chem.* **1992**, *31*, 5172.
- [2] B. Agboola, T. Nyokong, *Electrochim. Acta*, DOI: 10.1016/j.electacta.2007.02.017.
- [3] J. Simon, T. Toupance, in *Supramolecular Technology* (Ed.: D. N. Reinhoudt), Pergamon, Exeter, **1996**, vol. 10.
- [4] G. de la Torre, T. Torres, F. Aquillo-Lopez, *Adv. Mater.* **1997**, *9*, 265.
- [5] N. Toshima, T. Tominaga, S. Kawamura, *Bull. Chem. Soc. Jpn.* **1996**, *69*, 245.
- [6] B. Lukas, J. Silver, D. Lovett, M. J. Cook, *Chem. Phys. Lett.* **1995**, *241*, 351.
- [7] Ş. Abdurrahmanoğlu, A. R. Özkaya, M. Bulut, Ö. Bekaroğlu, *Dalton Trans.* **2004**, 4022.
- [8] H. Eichhorn, D. Wöhrle, D. Pressner, *Liq. Cryst.* **1997**, *22*, 643.
- [9] D. Lelievre, M. A. Petit, J. Simon, *Liq. Cryst.* **1989**, *4*, 707.
- [10] C. C. Leznoff, A. B. P. Lever, *Phthalocyanines: Properties and Applications*, VCH, New York, **1996**, vols. 1–4.
- [11] Ö. Bekaroğlu, *Appl. Organomet. Chem.* **1996**, *10*, 605 and references cited therein.
- [12] N. Kobayashi, H. Lam, W. A. Nevin, P. Janda, C. C. Leznoff, T. Koyama, A. Monden, H. Shirai, *J. Am. Chem. Soc.* **1994**, *116*, 879.
- [13] Y. Lemest, M. Lher, N. H. Hendricks, K. Kim, J. P. Collman, *Inorg. Chem.* **1992**, *31*, 835.
- [14] J. P. Collman, J. E. Hutchison, M. A. Lopez, A. Tabard, R. Guillard, W. K. Seok, J. A. Ibers, M. Lher, *J. Am. Chem. Soc.* **1992**, *114*, 9869.
- [15] N. Kobayashi, *Coord. Chem. Rev.* **2002**, *227*, 129.
- [16] N. Kobayashi, H. Lam, W. A. Nevin, P. Janda, C. C. Leznoff, A. B. P. Lever, *Inorg. Chem.* **1990**, *29*, 3415.
- [17] N. Kobayashi, Y. Yanagisawa, T. Osa, H. Lam, C. C. Leznoff, *Anal. Sci.* **1990**, *6*, 813.
- [18] Z. Odabaş, A. Altındal, A. R. Özkaya, B. Salih, Ö. Bekaroğlu, *Polyhedron* **2007**, *26*, 695.
- [19] D. Wöhrle, L. Kreienhoop, G. Schnurpfeil, J. Elbe, B. Tennigkeit, S. Hiller, D. Schlettwein, *J. Mater. Chem.* **1995**, *5*, 1819.
- [20] A. Altındal, Z. Z. Öztürk, S. Dabak, Ö. Bekaroğlu, *Sens. Actuators B* **2001**, *77*, 389.
- [21] D. Hohnholz, S. Steinbrecher, M. Hanack, *J. Mol. Struct.* **2000**, *521*, 231.
- [22] R. Murdey, N. Sato, M. Bouvet, *Mol. Cryst. Liq. Cryst.* **2006**, *455*, 211.
- [23] A. Y. Tolbin, A. V. Ivanov, L. G. Tomilova, N. S. Zefirov, *Mendeleev Commun.* **2002**, 96.
- [24] A. Y. Tolbin, A. V. Ivanov, L. G. Tomilova, N. S. Zefirov, *J. Porphyr. Phthalocyanines* **2003**, *7*, 162.
- [25] T. Ceyhan, A. Altındal, A. R. Özkaya, M. K. Erbil, B. Salih, Ö. Bekaroğlu, *Chem. Commun.* **2006**, 320.
- [26] C. H. Issidorides, R. Gulen, *Org. Synth.* **1963**, *Coll. vol. IV*, 679.
- [27] N. G. Lukyanenko, O. T. Melnik, T. I. Kirichenko, *Synth. Commun.* **1986**, *16*, 930.
- [28] V. Manivannan, W. A. Nevin, C. C. Leznoff, A. B. P. Lever, *J. Coord. Chem.* **1988**, *19*, 139.
- [29] J. R. Darwent, I. McCubbin, G. Porter, *J. Chem. Soc. Faraday Trans. 2* **1982**, *78*, 903.
- [30] N. Ishikawa, O. Ohno, Y. Kaizu, H. Kobayashi, *J. Phys. Chem.* **1992**, *96*, 8832.
- [31] D. Wöhrle, A. Wendt, A. Weitemeyer, J. Stark, W. Spiller, G. Schneider, S. Müller, U. Michelsen, H. Kliesch, A. Heuermann, A. Ardeschirpur, *Russ. Chem. Bull.* **1994**, *43*, 1953.
- [32] M. Özer, A. Altındal, A. R. Özkaya, M. Bulut, Ö. Bekaroğlu, *Synth. Met.* **2005**, *155*, 222.
- [33] A. B. P. Lever, E. R. Milaeva, G. Speier, in *Phthalocyanines: Properties and Applications* (Eds.: C. C. Leznoff, A. B. P. Lever), VCH Publishers, New York, **1993**, vol. 3.
- [34] W. A. Nevin, W. Liu, S. Greenberg, M. R. Hempstead, S. M. Marcuccio, M. Melnik, C. C. Leznoff, A. B. P. Lever, *Inorg. Chem.* **1987**, *26*, 891.
- [35] M. J. Stillman, A. J. Thompson, *J. Chem. Soc. Faraday Trans. 2* **1974**, *70*, 790.
- [36] C. C. Leznoff, S. M. Marcuccio, S. Greenberg, A. B. P. Lever, K. B. Tomer, *Can. J. Chem.* **1985**, *63*, 623.
- [37] W. A. Nevin, M. R. Hempstead, W. Liu, C. C. Leznoff, A. B. P. Lever, *Inorg. Chem.* **1987**, *26*, 570.
- [38] W. K. Lee, J. F. Liu, S. Walker, *Phys. Rev. Lett.* **1991**, *67*, 1559.

Received: January 31, 2007

Published Online: June 19, 2007